MODAL DECOMPOSITION FOR THIN-WALLED MEMBER STABILITY USING THE FINITE STRIP METHOD

B.W. Schafer
Johns Hopkins University, Department of Civil Engineering
Latrobe Hall 210, Baltimore, MD 21218, USA
E-mail: schafer@jhu.edu

S. Ádány
Budapest University of Technology and Economics, Department of Structural Mechanics
1111 Budapest, Műegyetem rkp. 3., Hungary
E-mail: sadany@epito.bme.hu

Abstract

This paper demonstrates how to decompose general stability solutions into useful subclasses of buckling modes through formal definition of the mechanical assumptions that underlie a class of buckling modes. For example, a thin-walled lipped channel column as typically used in cold-formed steel can have its buckling mode response decomposed into local, distortional, global, and other (transverse shear and extension) modes. The solution is performed by writing a series of constraint equations that are consistent with the mechanical assumptions of a given buckling class. The mechanical assumptions that defined the buckling classes were determined so as to be consistent with those used in Generalized Beam Theory (see e.g., Silvestre and Camotim 2002a,b) The resulting constraint equations may be used to constrain the solution before analysis, and thereby provide the opportunity to perform significant model reduction, or may be employed after the analysis to identify the buckling classes that participate in a given buckling mode. This paper shows the framework for this process in the context of the finite strip method (building off of Ádány and Schafer 2004, 2005a,b) and discusses some of the interesting outcomes that result from the application of this approach. Of particular interest, and discussed here, is the definition of global buckling modes, and the treatment of members with rounded corners – each of which provide certain challenges with respect to traditional definitions of the buckling classes. Examples are provided to illustrate the technique and challenges. The long-term goal of the work is to implement the procedures in general purpose finite element codes and thus enable modal decomposition to become a widely available tool for analyzing thin-walled member cross-section stability.

Introduction

Understanding cross-section stability of thin-walled members is critical to successful design. Inherently, or explicitly, design methods rely on prediction and separation of the cross-section stability modes. Different post-buckling behavior and strength are associated with each of the modes. For example, in the case of a cold-formed steel lipped channel column, typically three buckling modes are identified: local, distortional, and global. Local buckling modes are most typically handled by effective width methods which empirically include the potential for post-buckling reserve. Global buckling modes, such as flexural-torsional buckling, are handled through empirical column curves and are combined with the local post-buckling result in some fashion to account for local-global interaction. Distortional buckling is treated by modified effective width's or a modified column curve. Regardless of the design approaches employed, a fundamental first step is identification and prediction of the elastic cross-section stability modes.

Member Stability Solutions by the Finite Strip Method

Cross-section stability of open thin-walled members may be readily examined using the finite strip method. In a conventional stability solution the member is modeled as an inter-connected series of

M. Pandey et al. (eds), Advances in Engineering Structures, Mechanics & Construction, 411–422.

strips, as highlighted in **Figure 1**. The nodal lines of the strips have four degrees of freedom (DOF) each. In the local coordinates of the strip, the membrane DOF (u_i,v_i) follow plane stress assumptions, while the bending DOF (w_i,θ_i) follow thin plate bending assumptions. The membrane DOF are allowed to vary linearly in the transverse direction, while the bending DOF vary as a cubic (i.e., the typical beam shape function). Longitudinal deformation typically employs a trigonometric function, in its simplest form a single half-sine wave is enforced. The strips are transformed to global coordinates and assembled in a conventional manner to form the global stiffness matrices. A complete discussion of the finite strip method is available in Cheung and Tham (1998) and explicit details for construction of the elastic and geometric stiffness matrices as used in the open source program CUFSM are available in Schafer (1997).

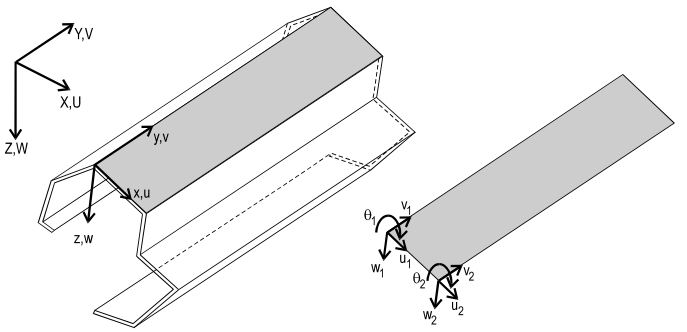

Figure 1. Coordinate systems and DOFs

The desired stability solution takes the form of an eigenvalue problem:

$$\mathbf{Kd} = \lambda \mathbf{K_g d} \tag{1}$$

where **K** is the global elastic stiffness matrix, $\mathbf{K_g}$ is the global geometric stiffness matrix, λ is the buckling load multipliers, and **d** is the buckling mode shapes. **K** is dependent on cross-section geometry and material, while $\mathbf{K_g}$ is dependent on geometry and the applied longitudinal stress. The size of the eigenvalue problem is equal to 4*n*, where *n* is the number of nodal lines. Since both **K** and $\mathbf{K_g}$ vary as a function of length, the conventional approach is to sweep through all lengths of practical interest and construct the FSM buckling load multiplier vs. half-wavelength curve. Alternatively, one could fix the length and instead sweep through all sine wave "frequencies" of interest; this is in essence the approach in a conventional finite element method (FEM) stability analysis.

As an example of the information gained from a typical FSM analysis, consider the C-section of example (a) as shown in **Figure 2**. The developed FSM model has numerous internal nodal lines to ensure the accuracy of the local buckling solution. The model has a total of 21 nodal lines, and thus 84 independent DOF. The eigenvalue problem size is thus 84x84. Further, the eigen solution is performed at 59 different lengths to generate the results of **Figure 2**b. The analysis results demonstrate FSM's ability to capture all cross-section stability modes of interest, from local plate instabilities to global member instability, and FSM provides a means to perform an initial classification. Based on the half-wavelength, the presence of minima, and the observed cross-section deformations, out of 84 possible buckling modes examined at 59 different lengths, three classes of buckling modes are approximately defined: local, distortional, and global.

FSM greatly reduces the problem size below a conventional FEM (shell/plate element) stability analysis. However, the further conceptual reduction of the solution (e.g., our 84x84 eigen problem solved 59 times) down to three buckling classes: local, distortional, and global, is necessary for design. Without this reduction the possibilities remain too numerous, and it is impractical to provide engineers with reasonable guidelines on the post-buckling and collapse response of all the modes. As detailed in

Schafer and Adany (2005) exceptions exist where the FSM analysis is not sufficient to definitively identify the classes. If the buckling classes are defined properly from the start it should be possible to perform the solution directly for classes of modes; instead of indirectly as is done in a conventional FSM analysis. In this way, the conceptual reduction performed at the conclusion of an FSM analysis could become a mechanical reduction performed at the beginning of an analysis.

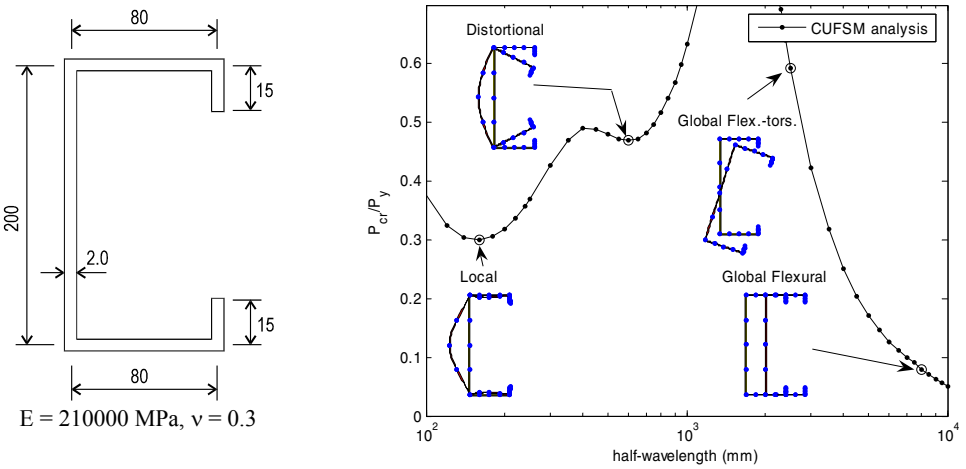

(a) example section (b) conventional finite strip method results

Figure 2. Finite strip analysis of a C-section with lips under pure compression, example (a)

Definition of Buckling Mode Classes

General

Generalized Beam Theory (GBT) is the only known method which is able to produce and isolate solutions for all the buckling modes: global, distortional and local. Further, modes identified via the GBT methodology are generally in accordance with commonly used definitions. Thus, our aim is to identify the critical assumptions in the GBT formulation that lead to the method's ability to isolate the modes. However, the goal is not to mimic the GBT formulation, but rather to construct the underlying GBT ideas as a series of distinct mechanical assumptions. These mechanical assumptions can then be enforced through constraints in more general methods such as FSM or FEM.

Mode Definitions

Based on an analysis of the GBT methodology, we put forth the following criteria as the critical mechanical assumptions necessary for defining the buckling modes. (Coord. system as in **Figure 1**.)

Criterion #1, membrane deformations:

- $\gamma_{xy} = 0$, membrane (in-plane) shear strains are zero,
- $\varepsilon_x = 0$, membrane transverse strains are zero, and
- $v = f(x)$, long. displacements are linear in x within an element/strip.

Criterion #2, longitudinal warping,

- $\varepsilon_y \neq 0$, long. strains/displacements are non-zero along the length.

Criterion #3, transverse flexure,

- $\kappa_y = 0$, no flexure in the transverse direction.

The buckling modes can then be defined as follows (see also Table 1).

- *Global* modes are those deformation patterns that satisfy all three criteria.
- *Distortional* modes are those deformation patterns that satisfy criteria #1 and #2, but do not satisfy criterion #3 (i.e., transverse flexure occurs).

- *Local* modes are those deformation patterns that satisfy criterion #1, but do not satisfy criterion #2 (i.e., no longitudinal warping occurs) while criterion #3 is irrelevant.
- *Other* modes are those deformations that do not satisfy criterion #1. Note, other modes do not exist in conventional GBT, but must exist in FSM due to the inclusion of membrane DOF.

Table 1. Mode classification table

	G modes	**D** modes	**L** modes	**O** modes
$\gamma_{xy} = 0$, $\varepsilon_x = 0$, v is linear	Yes	Yes	Yes	No
$\varepsilon_y \neq 0$	Yes	Yes	No	-
$\kappa_y = 0$	Yes	No	-	-

Modal Decomposition and the Constrained Finite Strip Method

General

The application of the above definitions implies that the appropriate deformation constraints, which are formulated in the three criteria, must be introduced into FSM. As a consequence, the original number of degrees of freedom (DOF) is necessarily reduced since the member can only deform in accordance with the strain conditions. Thus, our goal is to work out how the DOFs are reduced due to the various strain assumptions, and how this DOF reduction can practically be handled. Although the derivations are not extremely complicated, they are much longer than the limits provided by this paper. For this reason, here only a small example will be presented to demonstrate the method, which, at the same time, highlights all the important features of the more general derivations. Complete derivations can be found in (Ádány and Schafer 2005a).

Constraint Matrix Derivation

Consider the membrane deformation of a single finite strip, as shown in **Figure 1**. If the longitudinal distributions are assumed to be sinusoidal, as in the classical implementations of FSM, e.g., in CUFSM, the displacements can be expressed as a product of the assumed shape functions and the nodal displacements.

$$u(x,y) = \left[\left(1-\frac{x}{b}\right) \quad \left(\frac{x}{b}\right)\right]\begin{bmatrix} u_1 \\ u_2 \end{bmatrix} \sin\frac{m\pi y}{a} \tag{2}$$

$$v(x,y) = \left[\left(1-\frac{x}{b}\right) \quad \left(\frac{x}{b}\right)\right]\begin{bmatrix} v_1 \\ v_2 \end{bmatrix} \cos\frac{m\pi y}{a} \tag{3}$$

where u_1, u_2, v_1, v_2 are the transverse and longitudinal nodal displacements, m is the number of half-sine waves in the longitudinal direction, and a and b are the length and width of the strip, respectively.

Let us now introduce the criteria for zero transverse membrane strains:

$$\varepsilon_x = \frac{\partial u}{\partial x} = 0 \tag{4}$$

Substituting Eq. (2) into Eq. (4):

$$\varepsilon_x = \frac{\partial u}{\partial x} = \frac{-u_1 + u_2}{b} \sin\frac{m\pi y}{a} = 0 \tag{5}$$

and since the sine function is generally not equal to zero, u_1 and u_2 must be equal to each other in order to satisfy the equality.

This implies that the transverse displacements of the strip's two nodal lines must be identical, which is a natural consequence of the zero transverse strain assumption. In practice, the identical u

displacements prevent those deformations where the two longitudinal edges of the strip are not parallel, as illustrated in Figure 4.

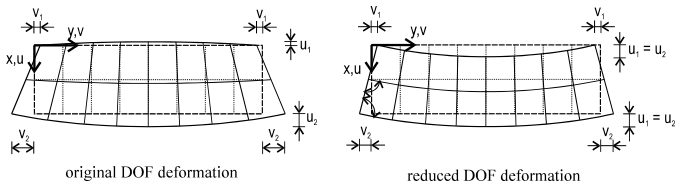

Figure 3. Effect of $\varepsilon_x = 0$ strain constraint on membrane deformations

The above derivation demonstrates that the introduction of a strain constraint reduces the number of DOFs, in this particular case from 4 to 3. Thus, we can define the new, reduced DOFs by u, v_1 and v_2, while the relationship of the original and reduced displacement vectors can be expressed as follows:

$$\begin{bmatrix} u_1 \\ v_1 \\ u_2 \\ v_2 \end{bmatrix} = \begin{bmatrix} 1 & 0 & 0 \\ 0 & 1 & 0 \\ 1 & 0 & 0 \\ 0 & 0 & 1 \end{bmatrix} \begin{bmatrix} u \\ v_1 \\ v_2 \end{bmatrix} \tag{6}$$

or in short:

$$\mathbf{d} = \mathbf{R}\mathbf{d}_\mathbf{r} \tag{7}$$

where **R** is the constraint matrix, which is a representation of the introduced strain constraints.

Constraint Matrix

In case of the more general strain-displacement constraints, and more general cross-sections, the derivations are somewhat more complicated, but finally the associated constraint matrices (**R**) can be defined, as shown in Ádány and Schafer (2005a,b) for G and D modes and Ádány (2004) for L and O modes, and thus apply for all the criterion summarized in Table 1. Since a different **R** matrix may be constructed for each of the modal classes: G, D, L, and O, taken together they span the entire original nodal basis and represent a transformation of the solution from the original nodal basis to a basis where G, D, L, and O deformation fields are segregated.

The columns of the **R** constraint matrices are the deformation fields associated with the G, D, L, and O spaces. For the C-section of example (a), modelled only with nodal lines at the corners and the free edge, making for a 24 DOF model, the columns of the **R** matrix are provided graphically in **Figure 4**. **Figure 4**a and b provide the warping displacements and transverse displacements for the G and D modes. An important characteristic of these modes is that the transverse displacements are uniquely defined by the warping displacements. **Figure 4**c provides the transverse displacements for the L modes (note, no warping occurs in the L modes). As shown in the figure, these L modes appear to be in the nodal DOF basis, but they are not identical to the original FSM nodal basis, because they represent only the part of the nodal rotations that meet the L constraints – note nodal rotations occur in the G and D modes as well. Finally, **Figure 4**d and e provide the O modes, associated with shear and transverse extension. As discussed in detail in Ádány and Schafer (2005a,b) additional transformation inside the G, D, L, O spaces are possible and desirable. One attractive option is to use unit-member axial modes as detailed in Ádány and Schafer (2005b). In many applications we are interest in only one mode class, and in such a case the **R** matrix truly represents a constraint on the original DOF and can be applied to reduce the problem size.

Applications for the Constrained Finite Strip Method

Pure Mode Calculation

By the application of constraints associated with the strain assumptions of the various modes as described in Table 1, the problem of pure buckling mode calculation can be solved. Instead of solving

the generalized eigenvalue problem of the member, as given in Eq. (1) one solves the reduced (or constrained) problem:

$$\mathbf{K_r d} = \lambda \mathbf{K_{gr} d} \tag{8}$$

where $\mathbf{K_r} = \mathbf{R}^T\mathbf{K}\mathbf{R}$ and $\mathbf{K_{gr}} = \mathbf{R}^T\mathbf{K_g}\mathbf{R}$ are the elastic and geometric stiffness matrix of the reduced DOF problem, respectively. **R** may be associated with any combination of the G, D, L, and O spaces or may include as little as one deformation field, for example D_1 of **Figure 4**, and thus reduce the problem to as little as one DOF.

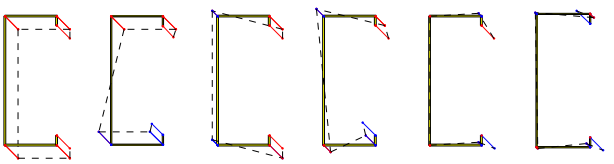

(a) warping displacements of G and D modes

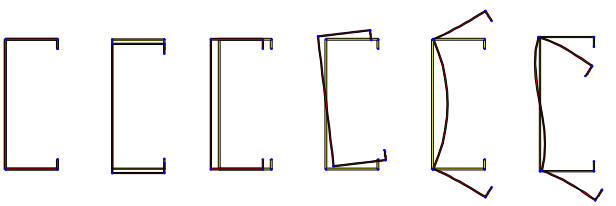

(b) transverse displacements of G and D modes

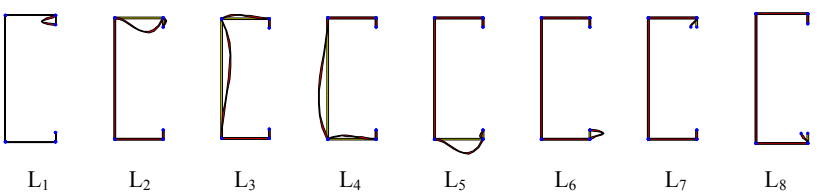

(c) transverse displacements of L modes (warping displacements are zero)

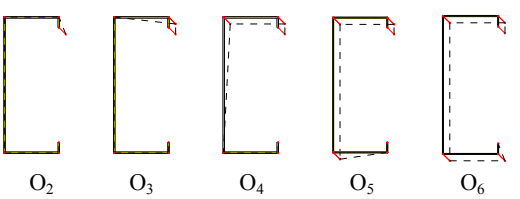

(d) warping displacement of O modes based on shear deformation (transverse displacements are zero)

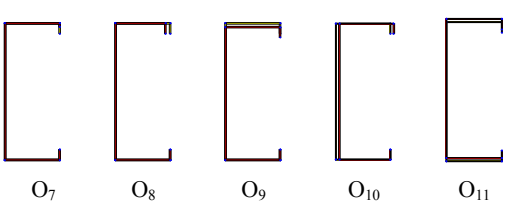

(e) transverse displacement of O modes based on transverse extension (warping displacements are zero)

Figure 4. Deformation modes of example (a) (nodal lines at fold lines only, model has 24 DOF)

To demonstrate the pure mode calculation results consider again the analysis of example (a). In **Figure 5**a the conventional FSM analysis is compared to three separate analyses, one constrained to the L

space, one constrained to the D space, and one constrained to the G space. The L space, spanned by the 8 deformation modes of **Figure 4**c requires solution of an 8x8 eigen problem. The D space, spanned by the last two deformation modes of **Figure 4**a and b requires solution of a 2x2 eigen problem, but actually the anti-symmetric D_2 mode does not contribute in this loading, so the solution can be simplified to a simple algebraic equation involving only the D_1 mode. The G space, spanned by the second through the fourth deformation modes of **Figure 4**a and b requires solution of a 3x3 eigen problem, and may be reduced to an algebraic equation for weak-axis flexural buckling and a 2x2 equation for flexural-torsional buckling. The constraint conditions successfully separate the modes.

The difference between the conventional FSM analysis and the D mode analysis is the most striking feature of the comparison. In **Figure 5**b the contribution of the L deformation modes and O deformation modes to this difference is demonstrated. Based on the mechanical definitions assumed here, the distortional minima in a conventional FSM analysis is not a pure mode; rather it includes interaction with additional mode classes; most notably, local buckling. Analysis of the combined LD space (9 DOF) provides a solution within ½% of the conventional FSM analysis (24 DOF). In this example the O modes must also be included (an additional 10 DOF) to close the error to zero. In other cross-sections distortional buckling may have a stronger interaction with global modes and thus the G space may be more important to include than the L space. No general conclusion can currently be made with regard to the significance of D modes which have interaction with L or G modes, but it is reasonable to assume that such a situation does impact the nature of the post-buckling response.

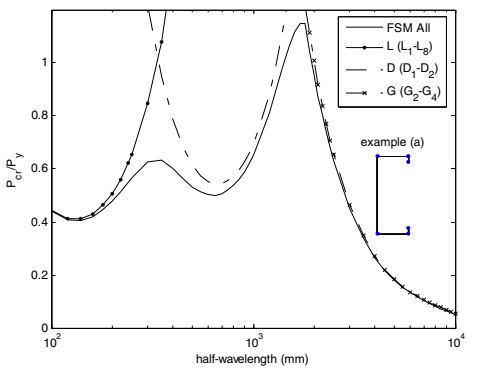

(a) FSM all mode analysis compared with constrained analyses in the L, D, and G mode classes

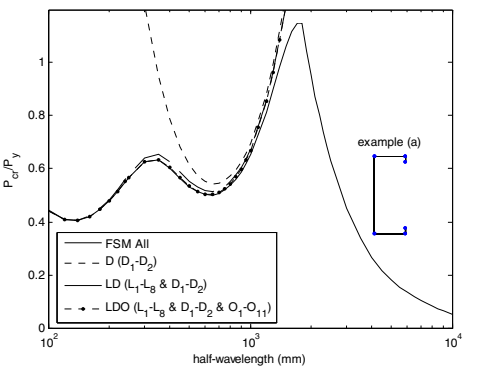

(b) FSM all mode analysis compared with constrained analysis in the D, D+L, and D+L+O mode classes

Figure 5. Comparison of conventional FSM analysis results with constrained models for example (a)

Mode Contribution Calculation

It is desirable to understand how the different pure modes of Eq. (8) for G, D, L, and O contribute in an all-mode or traditional FSM calculation, i.e. Eq. (1). This may be completed by transforming any displaced shape (buckled mode shape) into the eigenbasis created by the pure mode solution of Eq. (8). The eigenvectors **d** from the solution to Eq. (8) fully describe the pure mode solutions. Eq. (7) provides transformation from (or to) the pure mode space to the original DOF space.

The basis vectors must be normalized. Here, we select a normalization so that each base vector is associated with unit strain energy. In practice, let us consider again the eigenvalue problem of the member, as defined by Eq. (1). Any orthogonalized base vector satisfies Eq. (1), thus, we may write:

$$\mathbf{K}\mathbf{d}_\mathbf{o} = \lambda \mathbf{K}_\mathbf{g}\mathbf{d}_\mathbf{o} \tag{9}$$

where $\mathbf{d}_\mathbf{o}$ denotes the orthogonalized base vector. By pre-multiplying Eq. (9) with ½$\mathbf{d}_\mathbf{o}^{\mathrm{T}}$:

$$\frac{1}{2}\mathbf{d}_\mathbf{o}^{\mathrm{T}}\mathbf{K}\mathbf{d}_\mathbf{o} = \frac{1}{2}\lambda \mathbf{d}_\mathbf{o}^{\mathrm{T}}\mathbf{K}_\mathbf{g}\mathbf{d}_\mathbf{o} \tag{10}$$

where the left-hand side of the equation is the elastic strain energy, which by scaling the $\mathbf{d_o}$ vector can be set to unity. Any displacement vector can now be expressed as a linear combination of the basis vectors, by solving the linear matrix-equation as follows:

$$\mathbf{D_o c = d} \tag{11}$$

where $\mathbf{D_o}$ is a square matrix constructed from the orthonormal $\mathbf{d_o}$ base vectors so that each column of $\mathbf{D_o}$ would be a base vector; $\mathbf{d}$ is the given general displacement vector, while $\mathbf{c}$ is a vector containing the coefficients which are to be calculated. The contribution of any individual mode can be calculated as the ratio of the coefficient of that mode and the sum of all the coefficients, as follows:

$$|c_i| \Big/ \sum_{\text{all}} |c_i| \tag{12}$$

Similarly, the contribution of a mode class can be defined as:

$$\sum_{\text{mode}} |c_i| \Big/ \sum_{\text{all}} |c_i| \tag{13}$$

These definitions are preliminary, and imperfect. Currently the modal contributions defined in this manner are not unique. However, from a heuristic standpoint, they have value in allowing for an exploration of the various modal contributions.

Figure 6 provides modal contribution results for the cross-section of example (a), following Eq. (13). Generally the figure indicates the extent to which the G, D, L, or O classes contribute to the deformations at a given half-wavelength. For example, at the location of the distortional minimum (second minima in the curve of **Figure 6**a) D is the dominant class, but contributions from the other classes are observed. The defined contributions are imperfect, as they do not directly reflect the deformations impact on the buckling load. For example, at the local minima both D and O classes would appear to provide a significant modal contribution, but the analysis of **Figure 5**a indicates that the L class can provide the buckling load with only small error. While a robust modal contribution factor still remains a topic of future work, the value of such a metric is illustrated in **Figure 6**.

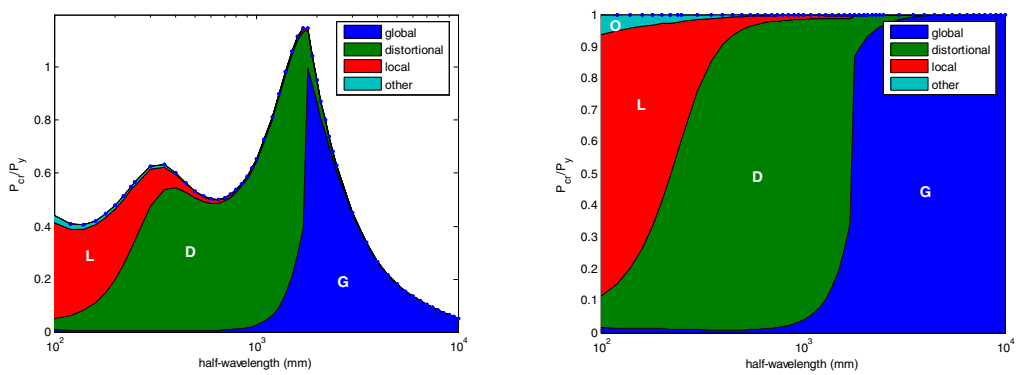

(a) under the conventional FSM analysis curve (b) as a simple portion of P_{cr}/P_y

Figure 6. Mode contribution/identification for example (a)

Discussion of Global Modes

A comparison of different solution methods for global modes highlight some important differences between constrained FSM, conventional FSM, and classically used analytical solutions. In **Figure 7**a the constrained FSM solution is compared to the classical analytical solution for flexural-torsional buckling (Timoshenko and Gere 1936). In the Figure, "Theory $G_1 - G_3$" represent the first three roots of the classical cubic equation that is solved for flexural-torsional buckling, and "$G_1 - G_3$" represent the first three eigenvalues of an FSM model constrained to only the deformations consistent with global modes (see **Figure 4**a and b). Constrained FSM gives higher critical forces. The difference is near 10% for any buckling lengths of practical importance. This difference is a direct consequence of the basic assumptions between beam and plate theory.

Constitutive Relations and Global Modes

In classical analytical solutions for global flexural buckling only the longitudinal normal stresses are considered, while the transverse normal stresses are assumed negligible. The problem is handled by a *beam model*, and only a one-dimensional constitutive relation, e.g.:

$$\begin{aligned}\sigma_x &= 0\\ \sigma_y &= E\varepsilon_y\\ \sigma_z &= 0\end{aligned} \tag{14}$$

Although rarely considered, transverse strains are not zero, even if they are small. FSM calculations are predicated on a *plate model*, and thus a two-dimensional constitutive relation, e.g.:

$$\begin{bmatrix}\sigma_x\\ \sigma_y\\ \tau_{xy}\end{bmatrix} = \begin{bmatrix}\frac{E}{1-\nu^2} & \frac{\nu E}{1-\nu^2} & 0\\ \frac{\nu E}{1-\nu^2} & \frac{E}{1-\nu^2} & 0\\ 0 & 0 & G\end{bmatrix}\begin{bmatrix}\varepsilon_x\\ \varepsilon_y\\ \gamma_{xy}\end{bmatrix} \tag{15}$$

It is assumed that the plates that form the cross-section are thin enough (compared to their width and length) that the Poisson effect should be considered. Thus, neither σ_x nor σ_y is negligible, while σ_z is implicitly assumed to be zero. If we calculate the pure global or distortional modes by applying the constraint matrix (**R**), we generate deformations that must satisfy the conditions that ε_x and γ_{xy} are zero. Thus, for constrained FSM the normal stresses can be expressed as follows:

$$\begin{aligned}\sigma_x &= \frac{\nu E}{1-\nu^2}\varepsilon_y\\ \sigma_y &= \frac{E}{1-\nu^2}\varepsilon_y\\ \sigma_z &= 0\end{aligned} \tag{16}$$

The difference between the beam model, Eq. (14), and the constrained FSM model, Eq. (16), is conspicuous. For longitudinal stresses the difference is equal to $1/(1-\nu^2)$. Considering that for steel the Poisson's ratio is approximately 0.3, the difference in the longitudinal stresses is approximately 10%. For flexural (global) buckling the only non-zero stress component (according to a beam model) is the longitudinal stress, consequently this difference in the longitudinal stresses directly transfers into a difference in the critical loads. The difference between the flexural buckling load calculated by the beam model and the constrained FSM is $1/(1-\nu^2)$ or 10% for ν=0.3. Flexural-torsional global buckling involves shear stresses which are not affected by the Poisson's ratio, therefore, a smaller difference (i.e., < 10%) occurs between analytical and constrained FSM solutions.

Classical Flexural-Torsional Buckling Beam Model

Although the beam model is the classical model of structural mechanics, applied for centuries, and at least for decades even in buckling problems, its application for thin-walled members can be regarded as only an approximation. Two important approximations are involved: (i) transverse stresses are neglected and (ii) transverse plate flexure is neglected.

To asses the consequence of neglecting the transverse stresses, let us consider the flexural buckling of Example (a). Either the column buckles about its minor or major axis. The majority of the elastic strain energy develops from membrane strains/stresses. If the plates that make up the member are slender enough, the plane stress assumption is certainly more reasonable than the 1D stress assumption, which means that the transverse stresses (Poisson effect) cannot be neglected. Thus, from this aspect the beam model *under-estimates* the column rigidity. Transverse flexure, though small in extent,

always takes place during flexural buckling. This may easily be demonstrated in a regular FSM or FEM analysis. It is obvious that transverse flexure provides additional flexibility to the column, consequently, from this aspect the beam model *over-estimates* the column rigidity. Thus, the beam model involves two competing approximations which nearly compensate each other so that the global buckling load provided by the beam model shows good agreement with more sophisticated models (e.g. FSM, see below) for most of practical cases, see **Figure 7**b.

Conventional FSM Model

A conventional FSM model (which is equivalent with a plate FEM model) considers both the Poisson effect and transverse plate flexure. If the analyzed plate elements are thin enough (which is always the case for cold-formed steel), and the applied finitization is sufficiently dense, both effects are considered in a correct way. Although these models still involve certain approximations (e.g. stresses/strains perpendicular to the plates are neglected), it is fair to say that FSM models calculate the elastic buckling of a thin-walled member with negligible error.

Constrained FSM Model

The constrained FSM model is a reduction of the regular FSM model, therefore it handles the plate elements as plates, i.e. together with the Poisson effect. However, the transverse strains as well as transverse flexure is completely eliminated, consequently a constrained FSM model behaves more rigidly than a regular FSM model. At the same time it differs from beam models, too, as already demonstrated via Eqs. (14) and (16), because it is not possible to simultaneously enforce zero transverse strains (which is a requirement from the basic GBT assumptions) and zero transverse stresses (which is the assumption of beam models). Since the constrained FSM satisfies the zero transverse strain condition, it gives larger rigidity, consequently higher critical forces than the beam models, as presented in **Figure 7**a.

Modified Constrained FSM

Unconstrained FSM provides the most rigorous solution, but does not allow decomposition nor identification of the buckling modes. Constrained FSM is clearly defined, but its lack of agreement with classical analytical solutions (the beam model) makes its practical use limited. Exact agreement between the beam model and constrained FSM is impossible. However, if we artificially assume that Poisson's ratio is zero, the constitutive equation for the constrained FSM model, Eq. (16) reduces to that of the beam model, Eq. (14). The two models are not identical, since transverse strains are zero in constrained FSM and non-zero in the beam model, but this difference has little effect, as **Figure 7**b shows.

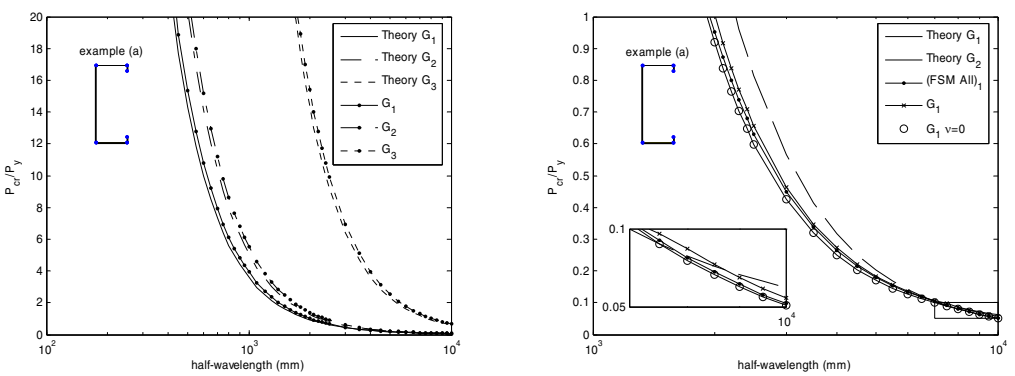

(a) analytical modes vs. pure global modes (b) comparison of global mode calculations

Figure 7. Comparison of global mode calculations for example (a)

The Impact of Corner Radii

In existing models with GBT the corners are always modeled as sharp, no corner radii is included. Comparison of FSM models with and without corner radii modeled, as shown in **Figure 8**a support the notion that the basic behavior is little influenced by small corner radii. A slight change in distortional buckling is observed, but this is still less than a few percent difference between the models.

However, from the standpoint of modal decomposition and the constrained FSM methods developed herein, the addition of corner radii has an important effect. **Figure 8**b illustrates the prediction of the local and distortional modes with three different models: an all mode, or conventional FSM analysis, and constrained models including only the D modes, and L modes. In addition, the figure also provides the predicted trasnverse displacements for the first minima (local buckling mode) predicted in the half-wavelength vs. buckling load plot. Even though the only change to the model is the addition of rounded corners, now the D modes do a better job of capturing the first minima than the L modes. Comparing this to the model with sharp corners of **Figure 5**a, the difference is striking. In fact, the predicted buckled shape via the L mode analysis is far too stiff when compared to a conventional (all mode) FSM analysis, and does not capture the appropriate deformations.

Comparing the transverse displacements in local buckling (**Figure 8**b); the L modes allow rotation only for the main nodes, and due to the angle changes around the corner all of the corner nodes are main nodes, thus the L modes effectively prevent the rotation of the corner as a global (rigid-body-like rotation). On the other hand, D modes allow transverse displacements, even though it is a special case of transverse flexure only, but since there are a many nodes in the vicinity of the corners, these transverse displacements result in a reasonable approximation of the real (all-mode) displacements. The addition of the corners also have a pronounced influence on the relationship between warping displacements and in-plane deformations. With the corners modeled explicitly, a gradient in the warping displacements through the corners allows a rotation to be engaged that closely mimics the corner rotations in the L modes of the sharp corner model. This may be best seen in the observed warping displacements, as given in **Figure 9**.

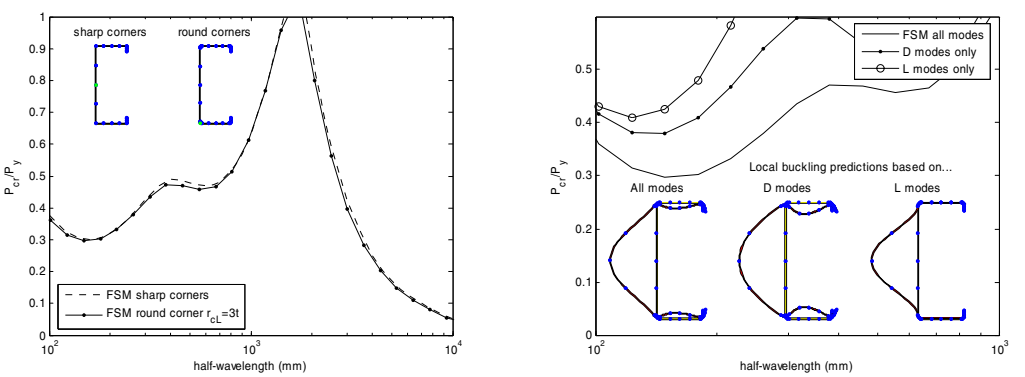

(a) FSM model results with sharp and round corners (b) decomposed model and predicted local modes

Figure 8. Impact of modeling cross-section with round corners on (a) FSM and (b) decomposition

The warping (longitudinal) displacements for the local buckling minima are provided in **Figure 9**. Comparison of **Figure 9**a and b, demonstrates that inclusion of corner radii alters the expected warping displacements. In a sharp corner model, the warping displacements only exist near the flange/lip juncture and have little impact on the actual result. With corner radii included in the model non-negligible warping also exists at the web/flange juncture; and further the warping distribution across the flange is approximately uniform. For constrained FSM models (**Figure 9**c and d) the D modes are unsuccessful in reproducing the actual (all mode) warping displacements, but the rounded corners allow warping at the web/flange juncture to engage bending in the web – and thus reasonably approximate the all mode local minima. Of course, the analysis consisting of L modes has, by definition, no warping, and in this case is a poor predictor.

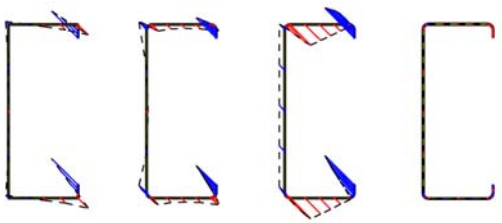

sharp corner round corner model
(a) all modes (b) all modes, (c) D modes (d) L modes

Figure 9. FSM predicted warping displacements for the local buckling minima

The constrained FSM method, based on GBT's mechanical assumptions, provides a unique means of decomposing a solution; however, it can not yet provide a general tool for modal classification and/or identification. The primary reason for this, is that reliance on heuristic definitions that describe the in-plane deformations; or simply point to minima in an FSM plot; are not themselves based on strict mechanical assumptions. Agreed upon definitions are needed in order to advance the field; however even simple issues such as models with corner radius included, demonstrate the challenges inherent in employing strict mechanical definitions. The corner radius models also suggest that further exploration of the relationship between criterion 3 regarding transverse flexure, and local plate bending are needed.

Conclusions

This paper provides an introduction to a new numerical method whereby general purpose finite element or finite strip methods can be constrained to deformation fields consistent with a particular class of buckling modes. The mechanical assumptions employed for this decomposition are based on Generalized Beam Theory, and implemented in a finite strip analysis. The decomposition (or constraining) of the conventional cross-section stability solution provides increased numerical efficiency and the potential to investigate cross-section stability behavior in a more detailed fashion. Some challenges exist when the approach is adopted; primarily related to the assumptions inherent in conventional solutions. For example, with global buckling modes it is shown that the constrained finite strip solutions are stiffer than analytic solutions due to the underlying constitutive relations. Models with and without corner radii present additional challenges for the mechanical definitions used to decompose the modes. Mechanics-based definitions of the cross-section stability modes do not agree well with current heuristic definitions when corner radii are present. Reasons for this difference are discussed in the paper. Modal decomposition brings the basic tools of Generalized Beam Theory for use in the more general finite strip method context, in doing so, both the advantages and limitations of such an approach are highlighted.

References

Ádány, S., Schafer, B.W. (2004). "Buckling mode classification of members with open thin-walled cross-sections." Fourth Int'l Conf. on Coupled Instabilities in Metal Structures, Rome, Italy, 27-29 Sept., 2004

Ádány, S., Schafer, B.W. (2005a). "Buckling mode decomposition of single-branched open cross-section members via finite strip method: derivation." Elsevier, *Thin-walled Structures*, (Submitted)

Ádány, S., Schafer, B.W. (2005b). "Buckling mode decomposition of single-branched open cross-section members via finite strip method: application and examples." Elsevier, *Thin-walled Structures*, (Submitted)

Cheung, Y.K., Tham, L.G. (1998). The Finite Strip Method. CRC Press.

Schafer, B.W. (1997). Cold-Formed Steel Behavior and Design: Analytical and Numerical Modeling of Elements and Members with Longitudinal Stiffeners. Ph.D. Disseration. Cornell University, Ithaca, NY.

Schafer, B.W., Ádány, S. (2005). "Understanding and classifying local, distortional and global buckling in open thin-walled members." Tech. Session and Mtg., Structural Stability Research Council. Montreal, Canada.

Silvestre, N., Camotim, D. (2002a). "First-order generalised beam theory for arbitrary orthotropic materials." *Thin-Walled Structures*, Elsevier, 40 (9) 755-789.

Silvestre, N., Camotim, D. (2002b). "Second-order generalised beam theory for arbitrary orthotropic materials." *Thin-Walled Structures*, Elsevier, 40 (9) 791-820.